Title

n-Type doping of a solution processed p-type semiconductor using isoelectronic surface dopants for homojunction fabrication

Authors

Mølnås, Håvard
Russ, Boris
Farrell, Steven L
et al.

Publication Date

2022-07-01

DOI

10.1016/j.apsusc.2022.153089

Peer reviewed

n-type Doping of a Solution Processed p-type Semiconductor for Homojunction Fabrication

*Håvard Mølnås[1], Boris Russ[2], Steven L. Farrell[1], Madeleine P. Gordon[2,3], Jeffrey J. Urban[2], and Ayaskanta Sahu[1]**

[1]Department of Chemical and Biomolecular Engineering, New York University, Brooklyn, New York 11201, USA.

[2]The Molecular Foundry, Lawrence Berkeley National Lab, 1 Cyclotron Road, Berkeley, CA 94720, USA.

[3]Applied Science and Technology Graduate Group, University of California, Berkeley, CA 94720, USA

KEYWORDS: Isoelectronic surface doping, p-n homojunction, solution processable, Bi_2Te_3 nanowires

Abstract: The p-n junction is one of the fundamental requirements for a practical semiconductor-based electronic device. Designing a heterojunction comprising of dissimilar p-type and n-type semiconductors calls for careful energy level considerations, both when selecting the semiconductor materials as well as the metal contacts. A homojunction based on a single semiconductor simplifies this task, as energy levels of the p-type and n-type materials are already

fairly similar, allowing for easier selection of contacts. Traditionally, homojunctions rely on doping of a bulk semiconductor to achieve p- and n-type transport through controlled addition of aliovalent dopants via energy-intensive processes such as ion implantation or thermal annealing. Exact control of doping in nanocrystalline semiconductors is significantly more challenging, due to self-purification effects. However, owing to their large surface areas, surface moieties can be utilized to both dope the nanostructures as well as tune their energy levels. In this report, we present a facile technique based on isoelectronic surface dopants in order to achieve p- and n-type materials based on the same semiconductor. We show that thin p-type colloidal Bi_2Te_3 nanowires can be switched to n-type through surface tuning, further extending the applicability of this technique and increasing the availability of new nanocrystalline solution-processable p-n homojunctions.

Introduction

Semiconductor electronic devices have revolutionized countless aspects of human life, from communication and automation to sustainable energy harvest and illumination[1-3]. Central to this development is the p-n junction, discovered by Russell Ohl in 1940[4]. Through its ability to direct charge flow, the p-n junction can be considered the elemental building block for a range of semiconductor devices, including light emitting diodes, solar cells and transistors. In 1st generation solar cells, positively and negatively doped bulk high purity silicon typically make up the p-type and n-type sides of the junction, respectively. However, with the increasing utilization of semiconductor devices in modern society, e.g. in the infrared or x-ray energy ranges inaccessible by silicon, the demand for p-n junctions comprised of increasingly exotic semiconductor materials is constantly on the rise.

When designing p-n junctions, great care must be taken to control charge densities of the p-type and n-type materials, as well as to match energy levels, in particular band edges. For bulk heterojunctions, where the p-type and n-type materials are based on different semiconductors, chemical compatibility and lattice matching are also very important in order to avoid heterojunction interface recombination and asymmetric expansion during traditional device assembly[5]. A homojunction, containing p-type and n-type materials based on the same semiconductor, simplifies many of these requirements, as lattice parameters and band edges already match while the Fermi level, E_F, varies slightly due to doping.

The selection of contacts is also greatly simplified for a homojunction. In a heterojunction, the difference in band gap between the p-type and n-type materials can be large, which could call for one contact with an extremely high work function and another contact with extremely low work function in order to inject and extract current. Metal contacts with very low work functions, such as calcium or strontium, are not very stable and are susceptible to oxidation[6]. A homojunction bypasses these challenges, and only requires contacts with work functions varying slightly around the band edges.

In bulk semiconductors, controlled addition of aliovalent dopants has become standard procedure in order to control charge density, for example through phosphorus or boron doping of high purity silicon through energy-intensive annealing. Albeit much utilized, this technique results in spatially inhomogeneous doping, and often introduces undesirable scattering mechanisms[7]. Another widely adopted technique is ion implantation, which can cause undesirable physical and chemical transformations in the host material owing to impingement of high energy dopant ions. This includes damage to or destruction of the crystal structure and even nuclear transmutations with ions of sufficiently high energy. However, there is limited band gap

flexibility when relying on only one bulk semiconductor, unless costly crystal growth methods are utilized to accurately control the chemical composition such as in mercury cadmium telluride, $Hg_{1-x}Cd_xTe$[8]. Bulk materials are also generally rigid, limiting usage of flexible surfaces.

The development of quantum confined nanomaterials opened a new avenue for controlling bandgaps in semiconductor materials[3, 9-11]. Available through solution-based synthesis, colloidal nanocrystals of a range of semiconductors can be fabricated with tremendous size and shape control, using less energy intensive techniques and at a lower cost than analogous methods. The ease of processability includes ease of upscaling and use of flexible substrates. However, although some band edge tuning has been demonstrated[12], controllable doping of these nanomaterials has proven to be challenging[13, 14].

In our previous work[7], we demonstrated interfacial sulfur doping of colloidal tellurium (Te) nanowires (NWs) as a remarkably straight-forward way to tune p-n type transport in a nanocrystalline semiconductor material. Through high-angle annular dark-field scanning transmission electron microscopy (HAADF-STEM), in combination with X-ray photoelectron spectroscopy (XPS) measurements and energy-dispersive X-ray (EDX) maps, we showed that sulfur dopant atoms are located primarily on the surface of the NWs. Through DFT calculations supported by ultraviolet photoelectron spectroscopy (UPS) studies, a mechanism was proposed where the surface sulfur dopants introduce a dopant band just below the conduction band of Te as well as a shift of the E_F from close to the valence band edge to the conduction band, resulting in n-type transport.

In this work, we revisit this facile surface engineering technique applied to more technologically relevant colloidal bismuth telluride (Bi_2Te_3) NWs and show that the p-n type transport can be controlled by surface doping with sulfur atoms for low diameter NWs. Bi_2Te_3

NWs were synthesized following a published route[15], and surface treatment followed the technique described by us[7]. As-synthesized and doped NWs were studied using a battery of techniques: Transmission electron microscopy (TEM), X-ray diffraction (XRD), energy-dispersive X-ray spectroscopy (EDS) and XPS was utilized to investigate changes in NW size, crystallinity, crystal structure and element distribution. Thermopower (Seebeck coefficient) and transistor measurements were conducted to evaluate the p-n transition. Our observations confirm the versatility of this surface engineering technique as a facile method to tune p-n type transport in a nanocrystalline colloidal semiconductor material.

Experimental section

Scheme 1. Synthesis and surface doping of Bi_2Te_3 NWs

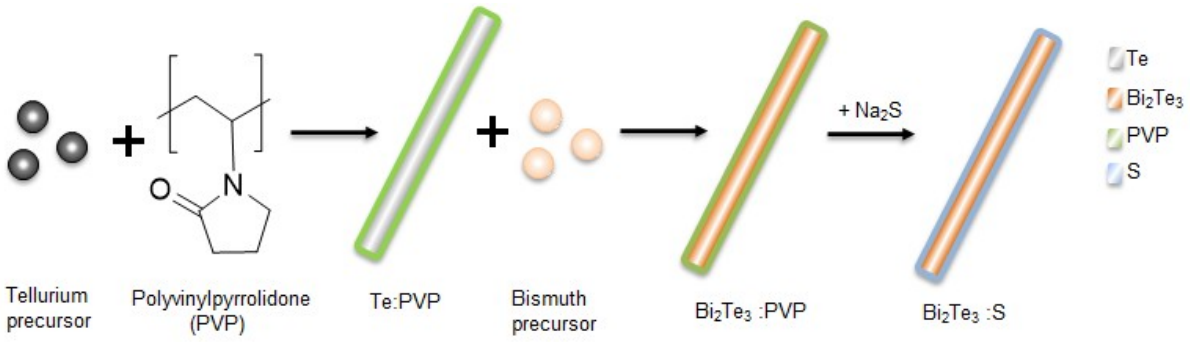

Chemicals and substrates. Tellurium dioxide (TeO_2, >99%), polyvinylpyrrolidone (PVP, M_W ~55 000), ethylene glycol (Emplura, >99%), sodium sulfide hydrate ($Na_2S{\cdot}xH_2O$, >60%) and methanol (reagent grade, 98%) were purchased from Sigma Aldrich. Sodium hydroxide (NaOH, 98%) was purchased from Alfa Aesar. Hydrazine hydrate (100%, 64.00-64.60% N_2H_4) and bismuth (III) nitrate pentahydrate ($Bi(NO_3)_3 \cdot 5H_2O$, 99.999%) were purchased from ACROS Organics. Acetone (J.T. Baker) and isopropyl alcohol (ACS Grade) were purchased from VWR

International. 1-ethyl-3-methylimidazolium bis(tri-fluoromethylsulfonyl)imide ([EMIM][TFSI]) was purchased from Solvent Innovation GmbH(Germany). All chemicals were used without further purification.

Glass substrates, 9.5 x 9.5 mm, and 0.2 mm thick, were purchased from Thin Film Devices. <100>-oriented, boron-doped Si wafers (resistivity = 0.005-0.01 Ω cm, thickness = 525 ± 25 μm) coated with 300 nm of thermal oxide (SiO_2) were purchased from Silicon Valley Microelectronics.

Synthesis of Bi_2Te_3 NWs. Synthesis and surface treatment are visualized in Scheme 1. 478.8 mg TeO_2, 600 mg NaOH and 200 mg PVP were added to 20 mL ethylene glycol in a three-neck flask in a standard Schlenk line setup, and heated to 160°C. Simultaneously, 818.5 mg $Bi(NO_3)_3 \cdot 5H_2O$ was dissolved in 5 mL ethylene glycol at 50°C in a separate vial. 1 mL hydrazine hydrate was injected as a reducing agent into the Te precursor at 160°C, and the Te NWs were grown for 1 hour. The Bi precursor was injected, and the reaction was run for an additional 1 hour. The reaction product was cooled naturally to room temperature, transferred to centrifuge tubes and diluted with 2 x 17.5 mL 18 MΩ distilled water and centrifuged at 8000 rpm and 5°C for 1 hour. The supernatant consisting of mainly amorphous Te and ethylene glycol was discarded, and the precipitate was cleaned an additional 3 times with 30 - 40 mL 18 MΩ distilled water.

Surface treatment of Bi_2Te_3 NWs. NWs were dispersed in 18 MΩ distilled water (4 - 5 mg/mL) and a 4 - 5x molar ratio of S^{2-} or HS^- ions to NWs was added with continuous stirring for up to ~24 hours. One experiment was extended using a fresh 10x mol ratio of S^{2-} for an additional ~51 hours. The ligand exchange progress was monitored through Seebeck coefficient measurements.

Characterization. X-ray diffraction, transmission electron microscopy, X-ray photoelectron spectroscopy and energy-dispersive X-ray spectroscopy were utilized to study the structure, size, shape and composition of the Bi_2Te_3 NWs.

A Bruker GADDS 8 microdiffractometer was used to collect wide-angle powder patterns (Cu-Kα). Nanocrystals films were deposited from concentrated Bi_2Te_3 in 18 MΩ water onto glass substrates or heavily doped Si wafers covered with a thermally grown 300 nm thick SiO_2 layer.

For TEM, a 200 kV FEI Titan Themis Scanning TEM, a 120 kV Libra120 and a 200 kV FEI Technai G20 Super Twin Lab6 microscope were used to image the NWs. The samples were prepared by depositing a drop of dilute NW dispersion in methanol onto a 300/400-mesh carbon coated copper grid followed by solvent evaporation at room temperature or 60°C.

XPS for examining Bi, Te, and S edges was performed using a Physical Electronics Versaprobe II XPS. Samples were prepared by drop casting NW suspensions in 18 MΩ water onto glass substrates and drying at 70°C for 10 min. Spectra were collected using an Al Kα source set to 49.4 W and 1.487 keV (250 meV resolution) with a 200 μm beam diameter. The survey pass energy was set to 117.40 eV, while the elemental pass energies were set to 29.35 eV. Prior to analysis, spectra were corrected by shifting the C1s peak to 284.8 eV.

EDS analyses were performed using a Zeiss Gemini Ultra-55 Analytical Field Emission Scanning Electron Microscope.

Ion gels. A symmetric poly(styrene-block-(ethylene oxide)-block-styrene)(PS-PEO-PS) triblock copolymer was synthesized as previously reported[16]. For ion gels, 1:9 (by weight) PS-PEO-PS and 1-ethyl-3-methylimidazolium bis(tri-fluoromethylsulfonyl)imide [EMIM][TFSI] were dissolved in dichloromethane (CH_2Cl_2). After stirring overnight, the solution was poured

into a Petri dish. CH_2Cl_2 was slowly evaporated at room temperature for 24 hours, and the ion-gel solution was further dried under vacuum for an additional 24 hours. Following complete evaporation of the solvent, transparent ion gels were formed, which were stored in a nitrogen filled glove box until needed.

Thermoelectric measurements. For thermoelectric, XRD and XPS measurements, quartz substrates were sonicated in acetone, isopropanol and methanol (10 minutes in each solvent), rinsed with methanol, dried at 100 °C for ~15 min and finally UV ozone treated for 30 min. 5 μm thick films of Bi_2Te_3 NWs were then drop-cast from a 100 mg/mL dispersion in water and heated at 70 °C for ~70 min. 100 nm Au contacts were patterned on the film by evaporation. A Keithley 2400 Sourcemeter in 4-wire Van-der-Pauw configuration was used to measure electrical conductivity. Seebeck coefficients (thermopower) were measured in a homemade setup consisting of two Peltier devices (Ferrotec) spaced ~4 mm apart. By driving current in opposing polarities through the devices, a temperature gradient resulted, varying with the magnitude of the current. Two T-type thermocouples mounted in micromanipulators were used to measure the temperature of the sample, and thermal contact was ensured by utilizing Si thermal paste (Wakefield Thermal S3 Solutions). The samples were typically exposed to five different temperature gradients, and ten voltage readings were recorded and averaged using an Agilent 34401 multimeter with an equilibration time of 2 - 3 minutes between temperature changes. Thermopower and conductivity data were acquired using homemade Labview programs. Measurement uncertainties of the Seebeck coefficient data were determined to roughly 2 - 3% and are hence captured within the data points unless otherwise noted. Uncertainty in electrical

conductivity data was on the order of 10 - 15%, originating from non-uniformity in film thickness.

Thin-film transistor measurements. Si/SiO_2 wafers sonicated in acetone, isopropanol, and methanol (10 minutes in each solvent), rinsed with methanol and dried at 100 °C for ~15 minutes were used as thin-film transistor substrates. ~100 - 200 nm thick films of Bi_2Te_3 NWs were either drop-cast from a 5 mg/ml dispersion in water and heated at 70 °C for ~30 minutes, or spin-coated (20 seconds at 1700 r.p.m. followed by 30 seconds at 3000 r.p.m.) from a 50 mg/ml dispersion in methanol and dried at room temperature for ~1 hour. 50 nm Au source and drain contacts were patterned on the film by evaporation. As the gate dielectric, an ion gel comprised of 9:1 by weight of the triblock copolymer PS-PEO-PS and of the ionic liquid [EMIM][TFSI], respectively, was spread over the active channel. Platinum foil placed over the ion gel served as the gate electrode. An Agilent 4155C semiconductor parameter analyzer was utilized to measure current-voltage (I-V) characteristics.

Results and Discussion

High resolution TEM analysis. Transmission electron micrographs in Figure 1 show undoped ~12 nm diameter Bi_2Te_3 NWs. The rough surfaces and polycrystalline domains of Bi_2Te_3, caused by introduction of Bi atoms into the original Te lattice during synthesis[15], are clearly visible, as well as a thin polymer layer.

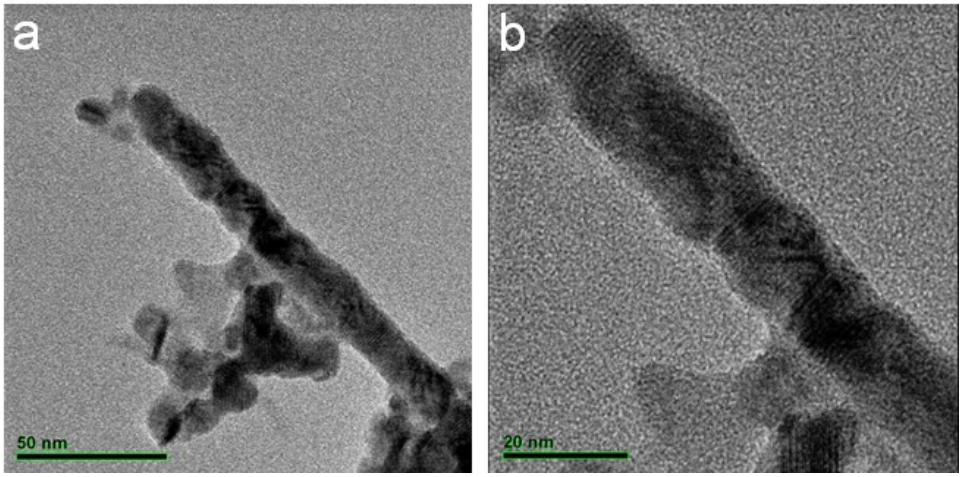

Figure 1. Transmission electron micrographs of undoped ~12 nm diameter Bi_2Te_3 NWs at different magnifications. The introduction of Bi atoms into the original Te lattice destroys the crystalline structure resulting in polycrystalline domains.

Figure 2 shows representative samples of thicker Bi_2Te_3 NWs before (a-b) and after (c-d) doping. The distribution of wire diameters is large, with an average NW diameter of 90 ± 20 nm. The polymer layer can be observed before S^{2-} treatment, but no evidence of any polymer is observed after, supporting the claim that S^{2-} atoms replace the polymer coating during the doping process. The replacement of polymer coating takes place through initial penetration of S^{2-} ions through the polymer layer and attachment to any unpassivated surface Te atoms. As more surface sites are exposed, the NW surface is gradually coated with S^{2-} atoms. The presence of surface Bi atoms in our Bi_2Te_3 NWs does not seem to prevent this exchange, resulting in complete removal of PVP after only 1 hour of S^{2-} treatment. The presence of Bi atoms can possibly lead to more favorable coordination with the sulfide ions. Regardless, we observe complete passivation with S^{2-} ions for both thin and thick wires. Additional images can be found in the Supplementary Information, Figure S1.

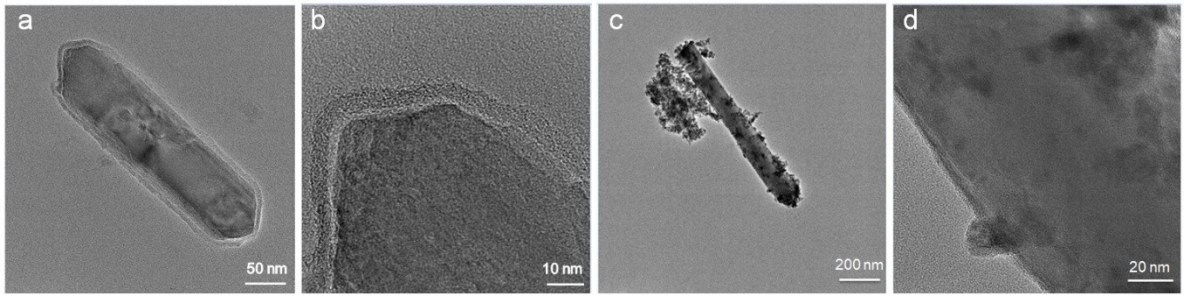

Figure 2. Transmission electron micrographs of undoped (a-b) and doped (c-d) 90 ± 20 nm diameter Bi_2Te_3 NWs. A thick polymer layer can be observed in a-b, while no evidence of any polymer can be observed in c-d.

XRD analysis. X-ray diffraction patterns of ~12 nm diameter NWs in Figure 3 show no significant change in the Bi_2Te_3 structure with 6 - 8 hours S^{2-} or HS^- doping. However, in contrast to Te NWs, with increased dopant concentration or time of reaction in Bi_2Te_3 NWs, we observe formation of mixed Bi_2Te_3-Bi_2S_3 phase, as shown for 90 ± 20 nm diameter NWs in Figure 4. We hypothesize that instead of simply attaching to the surface of the wires, owing to their small sizes, the sulfide ions can easily permeate into the Bi_2Te_3 lattice and replace some of the Te atoms.

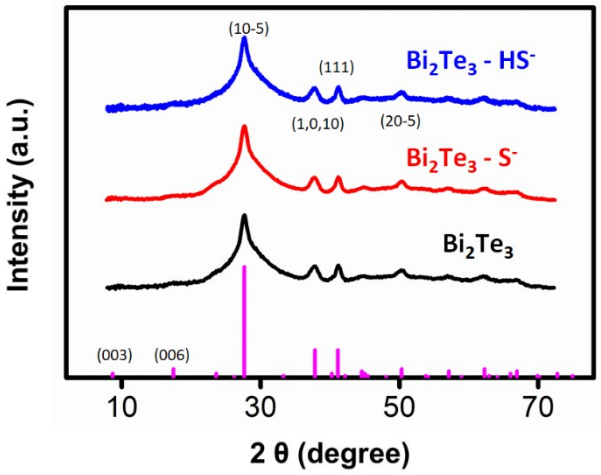

Figure 3. X-ray diffraction patterns for ~12 nm diameter undoped (black) and doped NWs (red – S^{2-}, blue HS^{-}). Purple bars denote reference peaks for pure Bi_2Te_3. The doping levels investigated do not alter the Bi_2Te_3 crystal structure of these small diameter NWs.

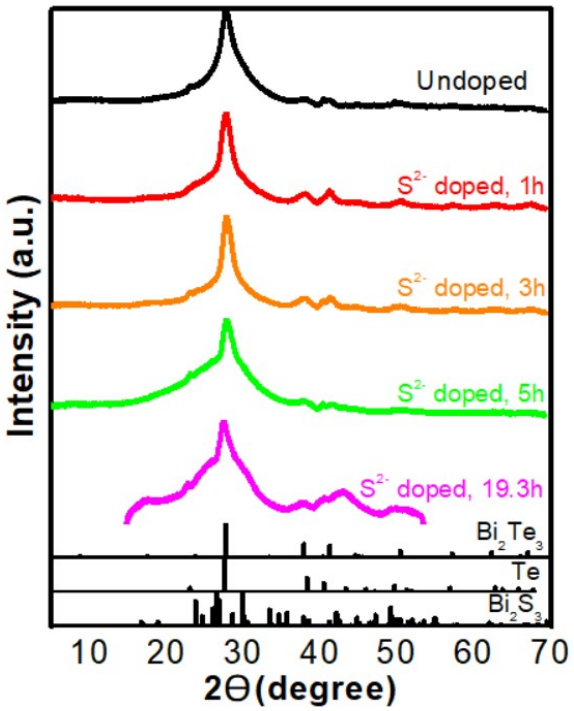

Figure 4. XRD patterns for undoped and S^{2-} doped ~90 nm diameter NWs compared to reference spectra for Bi_2Te_3 (ICSD 618187), Te (ICSD 161690) and Bi_2S_3 (ICSD 153952). Increased peak broadness is observed with increasing S^{2-} treatment time, indicating increased polycrystallinity, likely due to sulfur diffusion into the lattice.

EDS analysis. Energy-dispersive X-ray spectroscopy was used to study the addition of sulfur to the surface of the 90 ± 20 nm diameter NWs. Raw data is shown in Supplementary Information, Figure S2. While some uncertainty associated with absolute elemental concentrations is expected from EDS analyses, relative concentrations can still give an indication of process trends. The untreated NW surface was shown to be Te-rich, with an average Te:Bi-ratio of 1.8:1 (expected value of 1.5:1). With increased S^{2-} treatment time, the Te:Bi-ratio decreased to <1:1 while the S:Bi-ratio increased to ~1:1, which corroborates with the observations from XRD spectroscopy that the S^{2-} ions are not only confined to the surface but are slowly diffusing into the NW and

replacing the Te atoms. The amount of surface bound oxygen also decreased after S^{2-} treatment, which points toward effective passivation of surface NW atoms.

XPS analysis. X-ray photoelectron spectroscopy was used to study the surface chemistry and nature of bonds of the undoped and doped 90 ± 20 nm diameter Bi_2Te_3 NWs. At the Te-edge, Figure 5a, peaks at ~572 eV and ~582 eV are characteristic of Bi_2Te_3 and peaks at ~575 eV and ~586 eV are characteristic of oxidized Bi_2Te_3[15, 17]. It can be observed that oxide peaks are dominating in the undoped sample but are reduced relative to the Bi_2Te_3 peaks in the S^{2-} doped samples. These observations are in line with our previous work[7], which concluded that S^{2-} treatment of Te NWs passivates dangling bonds and suppresses surface oxidation. All peaks at the Te-edge are blue-shifted in the sample exposed to S^{2-} for 19.3 hours compared to the other two samples. This indicates a marginally more p-type material in the S-doped sample.

At the Bi-edge, Figure 5b, peaks at ~162.5 eV and ~157.2 eV are in good agreement with Bi_2Te_3[15, 18], while peaks at ~163.5 eV and ~158 eV indicate possible surface oxidation. It is observed that peaks in the sample S^{2-} treated for 1 hour match well with Bi_2Te_3, while the undoped sample and the sample S^{2-} treated for 19.3 hours match better with surface oxidation. The relative intensity of the peaks is the same in all three samples. Due to the proximity of the reference peaks and the resolution of the instrument, it is likely that what we observe is a convolution of both Bi_2Te_3 and Bi_2O_3 peaks, and that the changes in peak position between samples are due to the different absolute intensities of Bi_2Te_3 and Bi_2O_3 peaks. As discussed for the Te edge, it is likely that the 1 hour S^{2-} treatment suppresses oxidation, thus a better match with Bi_2Te_3 peaks at the Bi edge. After 19.3 h, the Bi_2O_3 peaks dominate since the surface is

again being oxidized, which can also be seen from the increased intensity of the oxide peaks at the Te edge after 19.3 h.

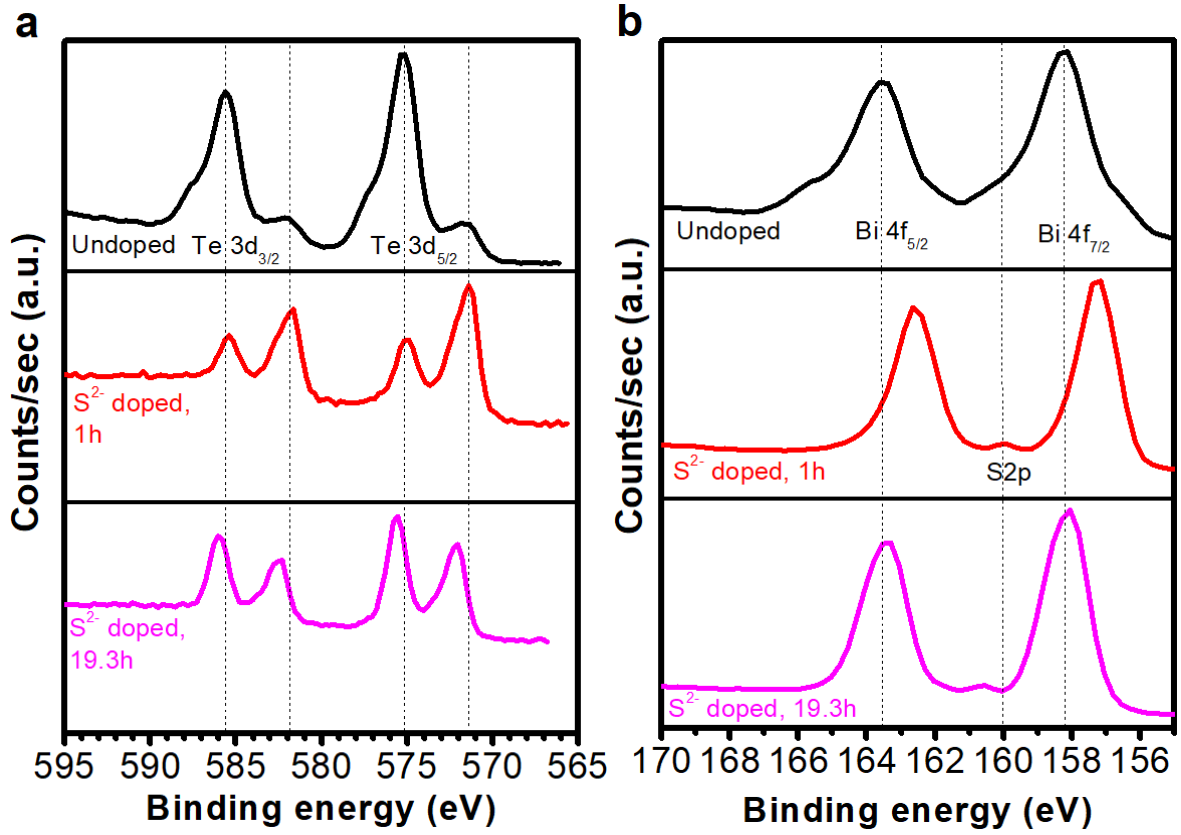

Figure 5. X-ray photoelectron spectra - tellurium edge (a) and bismuth/sulfur edges (b). The dotted vertical lines serve as guides for the eyes to visualize peak shifting. Suppression of surface oxidation after 1 hour S^{2-} treatment can be observed as a significant shift in relative intensities of peaks at the Te edge. The red/blue shifting of convoluted peaks at the Bi edge indicates an initial suppression, but eventual reappearance, of surface oxidation. The appearance of a S2p peak at the Bi edge after S^{2-} treatment indicates sulfide species on the surface.

Additionally, a new peak appears ~160 eV after S^{2-} treatment, and the peak is slightly blue shifted with increasing S^{2-} treatment time. This is likely the S2p peak indicative of sulfide species on the surface. Alternatively, the peak appearing at ~160 eV could be matched with a Bi_2S_3 $4f_{7/2}$ peak[18], although the absence of contributions from a corresponding Bi_2S_3 $4f_{5/2}$ peak at ~164 eV rules out large-scale formation of Bi_2S_3 close to the surface. We hypothesize that small polycrystallites of Bi_2S_3 might exist on the surface with no significant long-range order. The

absence of Te 4s peaks in the range 168 - 170 eV indicates that the introduction of Bi into the Te NWs during synthesis was successful such that no pure Te NWs remain.

Charge transfer analysis. Thermopower (Seebeck coefficient) and transistor measurements were conducted to evaluate the p-n transition. Figure 6 shows the calculated Seebeck coefficient (S) as the linear fit of the slope of open current voltage (V_{OC}) measurements at temperature gradients of ±15 K for undoped and doped ~12 nm diameter Bi_2Te_3 NWs. A shift from p-type to n-type transport can be observed with doping through the reversal of the sign of the Seebeck coefficient. This can be explained based on a starting position of the E_F well within the bandgap, but slightly closer to the valence band of undoped Bi_2Te_3 NWs. Due to S^{2-} surface doping, the charge carrier concentration is lowered, which leads to a decrease in the Seebeck coefficient and ultimately a sign change due to a bipolar effect[7]. A corresponding decrease in the electrical conductivity is also observed, which is a result of the decreased effective charge carrier concentration: As the sample becomes n-type doped, added electrons negate the majority holes in the originally p-type material until electrons start to dominate charge transport in the n-type material. A slight increase in electrical conductivity and absolute Seebeck coefficient is observed from HS^- doping to S^{2-} doping, indicating that S^{2-} is more effective at introducing electrons to the system, thus moving the E_F closer to the conduction band.

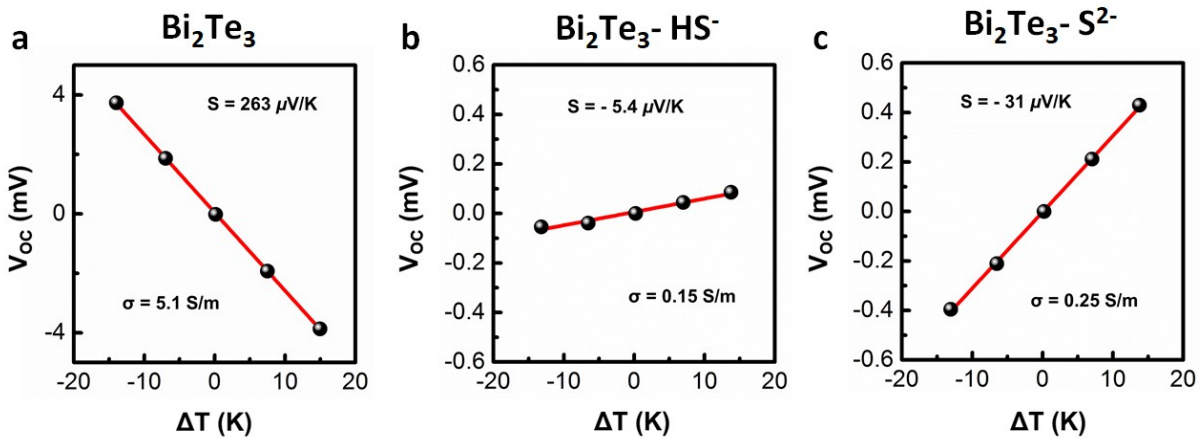

Figure 6. Thermoelectric transport properties for undoped (a), HS^- doped (b) and S^{2-}-doped (c) ~12 nm diameter Bi_2Te_3 NWs. The Seebeck coefficient (S) is calculated as the slope of the linear fit. A shift from p-type to n-type transport is observed with doping with reversal of the sign of S. A corresponding decrease in electrical conductivity, σ, is also observed.

Figure 7a-b show the average Seebeck coefficients at room temperature for 90 ± 20 nm diameter Bi_2Te_3 NWs as a function of exposure time to S^{2-}. For these thicker NWs, a shift from positive to negative Seebeck coefficient is not observed, even with increased S^{2-} concentration, indicating that the change in carrier concentration due to S^{2-} surface doping is not enough to shift the overall transport properties of the NWs from p-type to n-type. This is likely due to the reduced surface-to-volume ratio of the thick NWs compared to the thinner NWs. Instead, the Seebeck coefficient increases with S^{2-} treatment time, indicating that the material becomes more p-type. This matches the observation of blue shifted peaks at the Te edge in Figure 5a, indicating a more p-type character[7].

As indicated by the XRD and EDS results in Figure 4 and Figure S2, respectively, sulfur could be diffusing into the NWs forming Bi_2S_3, which in bulk is known to be an n-type semiconductor[19]. However, since a shift to n-type is not observed even at long S^{2-} treatment times

and increased dopant concentration, the anion exchange does not reach completion under these experimental conditions.

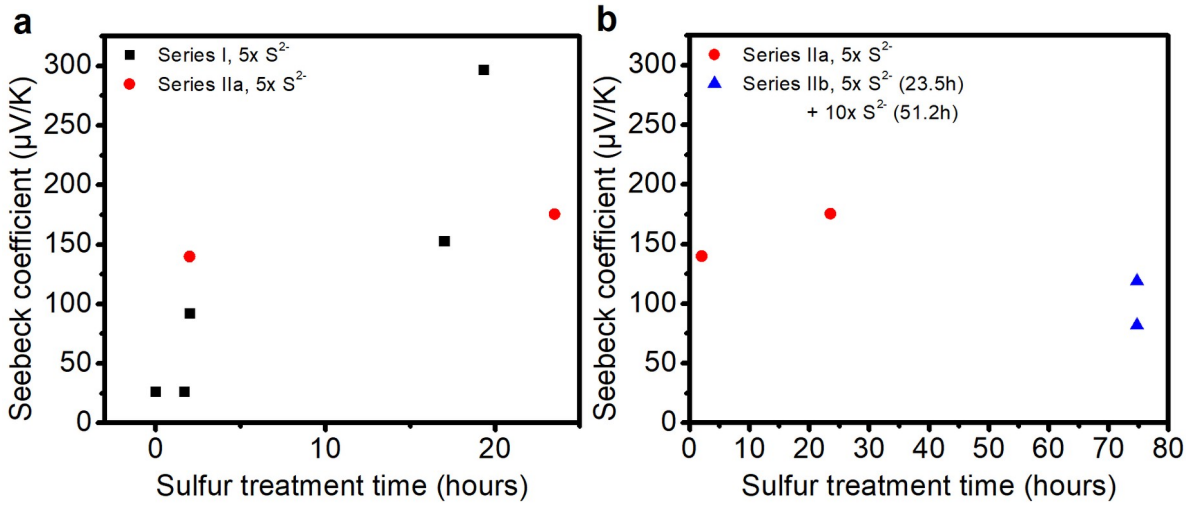

Figure 7. Seebeck coefficient as a function of sulfur treatment time for 90 ± 20 nm diameter Bi_2Te_3 NWs. Series I (black) and Series IIa (red) samples were exposed to a 5x S^{2-} mol concentration relative to NW concentration in 18 MΩ H_2O, while Series IIb (blue) samples were exposed to 5x S^{2-} for the first 23.5 hours and fresh 10x S^{2-} for the remaining 51.2 hours. Increased Seebeck coefficients are observed with increased S^{2-} treatment time for these thick NWs.

Having shown via open-circuit Seebeck measurements that the p-n transition in ~12 nm diameter Bi_2Te_3 NWs can be controlled via doping, an important criterion for possible use in diodes or transistors is to demonstrate that the material maintains the dominant charge carrier under bias. Electrolyte-gated thin-film transistor measurements were performed probing undoped and doped low diameter NW films under varying electrochemical potentials, shown schematically in Figure 8a. Figure 8c-d shows output and transfer characteristics for transistors made from undoped thin Bi_2Te_3 NWs. p-type (hole) charge transport is confirmed through the observation of sharply increasing drain current, I_D, with negative interface potential, V_G. In a similar fashion it can be concluded based on Figure 8e-f that S^{2-} doped thin Bi_2Te_3 NWs exhibit n-type charge transport, as I_D increases sharply with positive V_G. This suggests that the E_F shifts

closer to the conduction band edge with S^{2-} doping, as illustrated in Figure 8b. The origin of this shift is likely due to the mechanism outlined in our previous work[7], where sulfur absorption on the surface of the NWs introduces a dopant band just below the conduction band and an upward shift of the E_F into this new band. However, this needs to be confirmed by additional DFT modeling.

Alternatively, in mercury sulfide (HgS) quantum dot literature, surface S^{2-} adsorbates have been used to control the energy levels and thus control p-type/n-type transport through energy band shifting[20]. Electronegative S^{2-} ligands attract electrons from the HgS dots, thus moving the energy levels up with respect to the environmental E_F, making the material less n-type. DFT calculations in our previous work[7] show that S^{2-} does attract electrons from Te, creating a negatively charged surface region around surface bound S^{2-} ions. However, as for Te NWs, a shift towards n-type transport was observed with sulfur treatment for thin Bi_2Te_3 NWs, indicating a different mechanism than described for HgS quantum dots.

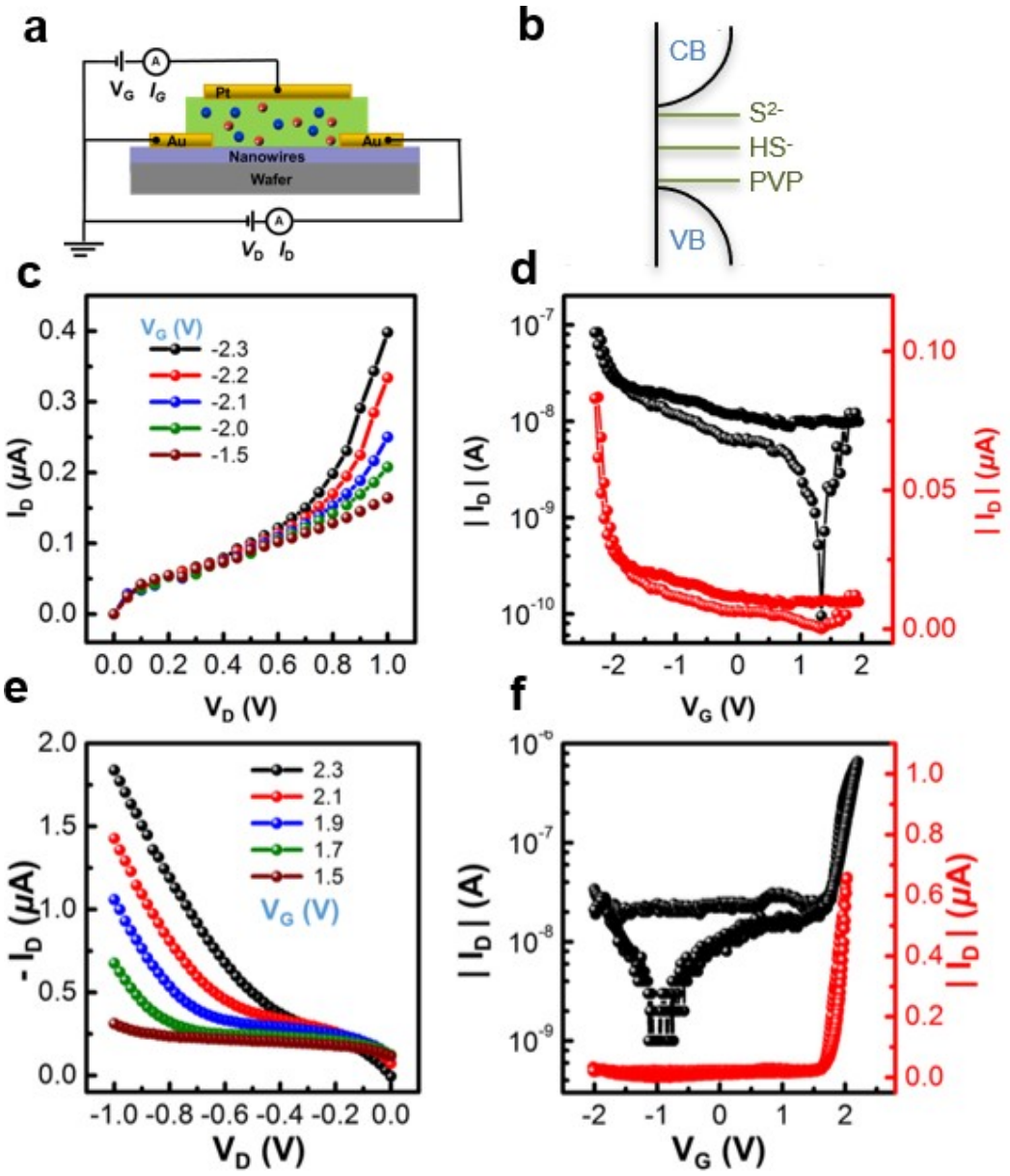

Figure 8. Fermi level shifts with doping. **a** Schematic cross section (not to scale) of ion-gel-gated thin-film transistors utilized to characterize the electrical properties of the ~12 nm diameter doped NWs. The length and width of the channel were 100 μm and 2 mm, respectively. Blue and red circles represent negative and positive ions, respectively. **b** Energy level diagram visualizing the proposed development of the Fermi energy (E_F) with respect to the band edges with and without sulfur doping. CB and VB refer to the conduction band and the valence band of Bi_2Te_3, respectively. **c** Output characteristics showing drain current, I_D, versus drain voltage V_D, for undoped ~12 nm diameter Bi_2Te_3 NWs at selected gate voltages (V_G) **d** Transfer characteristics for the undoped NW sample in **c** with V_D = 0.5 V, plotted on logarithmic and linear scales, as black and red curves, respectively, showing p-type transport. **e** Output characteristics showing I_D versus V_D, for S^{2-} doped ~12 nm diameter Bi_2Te_3 NWs at selected V_G. **d** Transfer characteristics for the doped NW sample in **e** with V_D = -0.5 V showing n-type transport.

Finally, for Bi_2Te_3 bulk single crystals prepared by Bridgman solidification[21], a switch from p-type to n-type was observed as a function of chemical composition; Te-rich (> 63%) being n-type and Bi-rich being p-type. p-n type switching was also demonstrated by electrodeposition; however, the correlation between stoichiometry and dominating charge transport did not always follow the straightforward compositional rule of thumb outlined above. Zhou et al.[22] varied electrolyte ratios to deposit p-type and n-type Bi_xTe_{1-x} NWs in nanoporous alumina, while Takahashi et al.[23] deposited p-type and n-type thin films by varying deposition potential. Other groups depositing Bi_2Te_3 thin films by sputtering[24, 25] also observed conflicting results with respect to chemical composition and suggested that p-type/n-type transport depends on crystal structure and more specifically the type of point defects in the lattice. On the nanoscale, Kim et al.[26] synthesized thick, Bi-rich, p-type Bi_2Te_3 nanotubes through a solution phase method diffusing Bi into Te NWs[27], while Zhang et al.[15] fabricated ultrathin, Te-rich, n-type Bi_2Te_3 NWs through an adapted colloidal route followed by removal of capping ligands by hydrazine treatment and sintering to a NW bulk pellet.

While p-n tuning of Bi_2Te_3 NWs has been shown previously through changing experimental synthesis conditions resulting in different chemical compositions and crystal structures, no clear consensus on the mechanism is reached. This work is the first to use our straightforward technique developed for Te NWs[7] to switch from p-type to n-type transport in Bi_2Te_3 NWs after synthesis while sustaining solution processability. The Bi_2Te_3 platform was utilized only to demonstrate feasibility of the technique, thus no optimization of thermoelectric performance was attempted. The possibility for further tuning of electrical transport properties of these Bi_2Te_3 NWs is expected, as well as expanding this method to other semiconductor materials.

Conclusions

Through this work we have extended the range of use of the facile surface doping technique first demonstrated for Te NWs to Bi_2Te_3 NWs and showed that isoelectronic surface dopants can be used to tune p-n type transport in this nanocrystalline semiconductor material. Thick and thin Bi_2Te_3 NWs were synthesized via a colloidal route, surface treated with S^{2-} or HS^- in an aqueous solution and characterized through a battery of techniques. XRD measurements showed that while the crystal structure of NWs was not adversely affected with moderate amounts of S^{2-} doping, extended periods of doping or large concentrations of S^{2-} ions lead to diffusion of dopant atoms into the lattice and replacement of native Te atoms leading to peak broadening. XPS demonstrated that S atoms at the surface of the NWs suppress oxidation, likely due to passivation of dangling bonds. Seebeck coefficient (thermopower) and transistor measurements confirmed a shift from p-type to n-type majority conduction in the thin NWs, while the thick NWs remained p-type. These results confirm the versatility of this surface engineering technique for p-n transport tuning for low diameter Bi_2Te_3 NWs, which could open the door to new p-n homojunction semiconductor devices in the future.

ASSOCIATED CONTENT

Supporting Information. Additional transmission electron micrographs of undoped thick Bi_2Te_3 NWs. EDS spectra of undoped and S^{2-} doped thick Bi_2Te_3 NWs. (PDF)

AUTHOR INFORMATION

Corresponding Author

***Ayaskanta Sahu** - Department of Chemical and Biomolecular Engineering, New York University, Brooklyn, New York 11201, USA. E-mail: asahu@nyu.edu

Authors

Håvard Mølnås - Department of Chemical and Biomolecular Engineering, New York University, Brooklyn, New York 11201, USA.

Boris Russ - The Molecular Foundry, Lawrence Berkeley National Lab, 1 Cyclotron Road, Berkeley, CA 94720, USA.

Steven L. Farrell - Department of Chemical and Biomolecular Engineering, New York University, Brooklyn, New York 11201, USA.

Madeleine P. Gordon – Applied Science and Technology Graduate Group, University of California, Berkeley, CA 94720, USA; The Molecular Foundry, Lawrence Berkeley National Lab, 1 Cyclotron Road, Berkeley, CA 94720, USA.

Jeffrey J. Urban - The Molecular Foundry, Lawrence Berkeley National Lab, 1 Cyclotron Road, Berkeley, CA 94720, USA.

ACKNOWLEDGMENT

The authors would like to acknowledge the Imaging Facility and Surface Science Facility of CUNY Advanced Science Research Center for instrument use, scientific and technical assistance. The authors acknowledge the use of shared facilities provided through the Materials Research Science and Engineering Center (MRSEC) program of the National Science Foundation under Award Numbers DMR-1420073 and DMR-0923251. Part of this work was performed at the Molecular Foundry, Lawrence Berkeley National Laboratory, and was supported by the Department of Energy, Office of Science, Office of Basic Energy Sciences, Scientific User Facilities Division of the U.S. Department of Energy under Contract No. DE-AC02-05CH11231. M.P.G. gratefully acknowledges support from the National Science Foundation Graduate Research Fellowship.

REFERENCES

1. Orton, J. W., *The Story of Semiconductors*. Oxford University Press: Oxford, 2008; p 528.

2. Łukasiak, L.; Jakubowski, A., History of Semiconductors. *Journal of Telecommunications and Information Technology* **2010,** (1), 3-9.

3. García de Arquer, F. P.; Talapin, D. V.; Klimov, V. I.; Arakawa, Y.; Bayer, M.; Sargent, E. H., Semiconductor quantum dots: Technological progress and future challenges. *Science* **2021,** *373* (6555), eaaz8541.

4. Ohl, R. S. Light-sensitive electric device. U.S. Patent US2402662A, May 27, 1941.

5. Fonash, S. J., Chapter Five - Semiconductor–semiconductor Heterojunction Cells. In *Solar Cell Device Physics (Second Edition)*, Fonash, S. J., Ed. Academic Press: Boston, 2010; pp 183-262.

6. Michaelson, H. B., The work function of the elements and its periodicity. *Journal of Applied Physics* **1977,** *48* (11), 4729-4733.

7. Sahu, A.; Russ, B.; Liu, M.; Yang, F.; Zaia, E. W.; Gordon, M. P.; Forster, J. D.; Zhang, Y.-Q.; Scott, M. C.; Persson, K. A.; Coates, N. E.; Segalman, R. A.; Urban, J. J., In-situ resonant band engineering of solution-processed semiconductors generates high performance n-type thermoelectric nano-inks. *Nature Communications* **2020,** *11* (1), 2069.

8. Lhuillier, E.; Guyot-Sionnest, P., Recent Progresses in Mid Infrared Nanocrystal Optoelectronics. 2017; Vol. 23, pp 1-8.

9. Carey, G. H.; Abdelhady, A. L.; Ning, Z.; Thon, S. M.; Bakr, O. M.; Sargent, E. H., Colloidal Quantum Dot Solar Cells. *Chemical reviews* **2015,** *115* (23), 12732-12763.

10. Murray, C. B.; Kagan, C. R.; Bawendi, M. G., Synthesis and Characterization of Monodisperse Nanocrystals and Close-Packed Nanocrystal Assemblies. *Annual Review of Materials Science* **2000,** *30* (1), 545-610.

11. Murray, C. B.; Sun, S.; Gaschler, W.; Doyle, H.; Betley, T. A.; Kagan, C. R., Colloidal synthesis of nanocrystals and nanocrystal superlattices. 2001; Vol. 45, pp 47-56.

12. Brown, P. R.; Kim, D.; Lunt, R. R.; Zhao, N.; Bawendi, M. G.; Grossman, J. C.; Bulović, V., Energy Level Modification in Lead Sulfide Quantum Dot Thin Films through Ligand Exchange. *ACS Nano* **2014,** *8* (6), 5863-5872.

13. Zunger, A.; Malyi, O. I., Understanding Doping of Quantum Materials. *Chemical reviews* **2021,** *121* (5), 3031-3060.

14. Norris, D. J.; Efros, A. L.; Erwin, S. C., Doped Nanocrystals. *Science* **2008,** *319* (5871), 1776.

15. Zhang, G.; Kirk, B.; Jauregui, L. A.; Yang, H.; Xu, X.; Chen, Y. P.; Wu, Y., Rational Synthesis of Ultrathin n-Type Bi2Te3 Nanowires with Enhanced Thermoelectric Properties. *Nano Letters* **2012,** *12* (1), 56-60.

16. Hadjichristidis, N.; Pispas, S.; Floudas, G., *Block Copolymers: Synthetic Strategies, Physical Properties, and Applications*. John Wiley & Sons: 2003.

17. Sun, T. S.; Buchner, S. P.; Byer, N. E., Oxide and interface properties of anodic films on Hg1−xCdxTe. *Journal of Vacuum Science and Technology* **1980,** *17* (5), 1067-1073.

18. Ismail, F. M.; Hanafi, Z. M., Some Physico-Chemical Properties of Bismuth Chalcogenides x-Ray Photoelectron and Diffuse Reflectance Spectra. *Zeitschrift für Physikalische Chemie* **1986,** *267O* (1), 667-672.

19. Madelung, O., *Semiconductors: Data Handbook*. 3 ed.; Springer-Verlag Berlin Heidelberg: 2004.

20. Jeong, K. S.; Deng, Z.; Keuleyan, S.; Liu, H.; Guyot-Sionnest, P., Air-Stable n-Doped Colloidal HgS Quantum Dots. *The Journal of Physical Chemistry Letters* **2014,** *5* (7), 1139-1143.

21. Fleurial, J. P.; Gailliard, L.; Triboulet, R.; Scherrer, H.; Scherrer, S., Thermal properties of high quality single crystals of bismuth telluride—Part I: Experimental characterization. *Journal of Physics and Chemistry of Solids* **1988,** *49* (10), 1237-1247.

22. Zhou, J.; Jin, C.; Seol, J. H.; Li, X.; Shi, L., Thermoelectric properties of individual electrodeposited bismuth telluride nanowires. *Applied Physics Letters* **2005,** *87* (13), 133109.

23. Takahashi, M.; Kojima, M.; Sato, S.; Ohnisi, N.; Nishiwaki, A.; Wakita, K.; Miyuki, T.; Ikeda, S.; Muramatsu, Y., Electric and thermoelectric properties of electrodeposited bismuth telluride (Bi2Te3) films. *Journal of Applied Physics* **2004,** *96* (10), 5582-5587.

24. Goto, M.; Sasaki, M.; Xu, Y.; Zhan, T.; Isoda, Y.; Shinohara, Y., Control of p-type and n-type thermoelectric properties of bismuth telluride thin films by combinatorial sputter coating technology. *Applied Surface Science* **2017,** *407*, 405-411.

25. Sudarshan, C.; Jayakumar, S.; Vaideki, K.; Sudakar, C., Te-rich Bi2Te3 thin films by electron−beam deposition: Structural, electrical, optical and thermoelectric properties. *Thin Solid Films* **2020,** *713*, 138355.

26. Kim, D.; Du, R.; Yu, S.-Y.; Yin, Y.; Dong, S.; Li, Q.; Mohney, S. E.; Li, X.; Tadigadapa, S., Enhanced thermoelectric efficiency in nanocrystalline bismuth telluride nanotubes. *Nanotechnology* **2020,** *31* (36), 365703.

27. Zhang, G.; Yu, Q.; Yao, Z.; Li, X., Large scale highly crystalline Bi2Te3nanotubes through solution phase nanoscale Kirkendall effect fabrication. *Chemical Communications* **2009,** (17), 2317-2319.